Silicon-on-insulator spectrometers with integrated GaInAsSb photodiodes for wide-band spectroscopy from 1510 to 2300 nm

E. Ryckeboer,[1,2,*] **A. Gassenq,**[1,2] **M. Muneeb,**[1,2] **N. Hattasan,**[1,2] **S. Pathak,**[1,2] **L. Cerutti,**[3] **J.B. Rodriguez,**[3] **E. Tournié,**[3] **W. Bogaerts,**[1,2] **R. Baets,**[1,2] **and G. Roelkens**[1,2]

[1] *Photonics Research Group, INTEC Department, Ghent University - IMEC, Sint-Pietersnieuwstraat 41,9000 Ghent, Belgium*

[2] *Center for Nano- and Biophotonics (NB-Photonics), Ghent University, Belgium*

[3] *Institut d'Electronique du Sud (IES), UMR 5214, Université Montpellier 2 - CNRS, F-34095 Montpellier cedex 5, France*

[*] *eva.ryckeboer@intec.ugent.be*

Abstract: We present a silicon-on-insulator (SOI) based spectrometer platform for a wide operational wavelength range. Both planar concave grating (PCG, also known as echelle grating) and arrayed waveguide grating (AWG) spectrometer designs are explored for operation in the short-wave infrared. In addition, a total of four planar concave gratings are designed to cover parts of the wavelength range from 1510 to 2300 nm. These passive wavelength demultiplexers are combined with GaInAsSb photodiodes. These photodiodes are heterogeneously integrated on SOI with benzocyclobutene (DVS-BCB) as an adhesive bonding layer. The uniformity of the photodiode characteristics and high processing yield, indicate a robust fabrication process. We demonstrate good performance of the miniature spectrometers over all operational wavelengths which paves the way to on-chip absorption spectroscopy in this wavelength range.

© 2013 Optical Society of America

OCIS codes: (130.3120) Integrated optics devices; (300.6190) Spectrometers.

References and links

1. M. C. Estevez, M. Alvarez, and L. M. Lechuga, "Integrated optical devices for lab-on-a-chip biosensing applications," Laser Photon. Rev. **6**(4), 463–487 (2012).
2. K. De Vos, I. Bartolozzi, E. Schacht, P. Bienstman, and R. Baets, "Silicon-on-insulator microring resonator for sensitive and label-free biosensing," Opt. Express **15**(12), 7610–7615 (2007).
3. J. Brouckaert, W. Bogaerts, S. Selvaraja, P. Dumon, R. Baets, and D. Van Thourhout, "Planar concave grating demultiplexer with high reflective bragg reflector facets," IEEE Photon. Technol. Lett. **20**(4), 309–311 (2008).
4. W. Bogaerts, S. Selvaraja, P. Dumon, J. Brouckaert, K. De Vos, D. Van Thourhout, and R. Baets, "Silicon-on-insulator spectral filters fabricated with CMOS technology," IEEE J. Sel. Top. Quantum Electron. **16**(1), 33–44 (2010).
5. J. G. Crowder, S. D. Smith, A. Vass, and J. Keddie, "Infrared methods for gas detection," *Mid-Infrared Semiconductor Optoelectronics.* (Springer-Verlag, 2006).
6. A. Amerov, J. Chen, and M. Arnold, "Molar absorptivities of glucose and other biological molecules in aqueous solutions over the first overtone and combination regions of the near-infrared spectrum," Appl. Spectrosc. **58**(10), 1195–1204 (2004).

7. A. Gassenq, N. Hattasan, E. M.P. Ryckeboer, J.B. Rodriguez, L. Cerutti, E. Tournié, and G. Roelkens, "Study of evanescently-coupled and grating-assisted GaInAsSb photodiodes integrated on a silicon photonic chip," Opt. Express **20**(11), 11665–11672 (2012).

8. http://www.epixfab.eu/.

9. M. K. Smit and C. Van Dam, "Phasar-based wdm-devices: principles, design and applications," IEEE J. Sel. Top. Quantum Electron. **2**(2), 236–250 (1996).

10. R. Marz. *Integrated Optics, Design and Modeling.* (Artech House Inc., 1994).

11. J. Brouckaert, W. Bogaerts, P. Dumon, D. Van Thourhout, and R. Baets, "Planar concave grating demultiplexer fabricated on a nanophotonic silicon-on-insulator platform," J. Lightwave Technol. **25**(5), 1269–1275 (2007).

12. A. C. Bedoya, M. Y. Ling, J. Brouckaert, N. A. Yebo, D. Van Thourhout, and R. Baets, "Biodiesel sensing using silicon-on-insulator technologies," Proc. SPIE, 7366, (2009).

13. G. J. Veldhuis, O. Parriaux, H. Hoekstra, and P. V. Lambeck, "Sensitivity enhancement in evanescent optical waveguide sensors," J. Lightwave Technol. **18**(5), 677–682 (2000).

14. A. Bauer, K. Rner, T. Lehnhardt, M. Kamp, S. Hfling, L. Worschech, and A. Forchel, "Mid-infrared semiconductor heterostructure lasers for gas sensing applications," Semicond. Sci. Technol. **26**(1), 4032 (2011).

1. Introduction

In recent years the interest for sensing of biological molecules with compact lab-on-a-chip systems is strongly increasing [1, 2]. An important and selective detection method is absorption spectroscopy. Nowadays, the standard equipment for absorption spectroscopy, UV-VIS-NIR spectrophotometers and FTIR, demonstrate high performance, but they are bulky and expensive. Integrated photonics offers an opportunity to miniaturize these spectrometers while maintaining high sensitivity. In this work, we explore integrated spectrometers fabricated on the silicon-on-insulator (SOI) platform, which enables a very small device footprint. Moreover, the fabrication of SOI chips is CMOS-compatible, thus allowing mass fabrication at low cost. From earlier device demonstrations in the telecommunication bands [3, 4], it is known that planar concave gratings (PCG) and arrayed waveguide gratings (AWG) are efficient and performant wavelength demultiplexers. By extending the operational range of these demultiplexers to the short wave infrared (SWIR), we can cover a broad wavelength range for spectroscopy. This enables a smaller detection limit as the absorption strength is typically stronger in the short-wave infrared [5]. In addition, by taking a wider spectrum, we can detect a larger variety of molecules while reducing the effect of interfering molecules. In this work, we present the results of an AWG and PCG designed for respectively 2.2 and 2.3 μm. Next to this demonstration of SWIR passive demultiplexers, we combine four planar concave grating designs on a single chip, each covering a distinct band between 1.51 and 2.3 μm, with GaInAsSb photodiodes. Using this wide wavelength range, the first overtone band of C-H stretching vibrations (1550-1850 nm) and the combination of stretching and bending vibrations of C-H, N-H and O-H bonds (2000-2500 nm) are covered, allowing the probing of a wide range of molecules and substances such as glucose and biodiesel [6]. The p-i-n photodetectors are heterogeneously integrated on the waveguide circuit by employing benzocyclobutene (DVS-BCB) as an adhesive bonding layer [7]. We use a quaternary GaInAsSb epitaxial layer stack, which has a bandgap wavelength of 2.65 μm at room temperature, as the active photodetector material. These photodetectors show good performance with responsivities up to 0.7 A/W, high processing yield and good uniformity. This paper is structured as follows: first, the wavelength demultiplexer designs are discussed. Secondly, detail is provided on the photodiode fabrication process and characteristics, after which we present the results of the spectrometers with integrated photodiodes to end with a conclusion and outlook.

2. Wavelength demultiplexer designs

In this section we discuss the demultiplexer designs of both arrayed waveguide gratings for 2.2 μm and four planar concave grating designs with respectively 1.55 μm, 1.65 μm, 2.12 μm,

2.32 μm as center wavelengths. The photonic chip containing the demultiplexers is fabricated in a CMOS pilot line on a 200 mm SOI wafer, comprising a 220 nm thick Si waveguide layer on a 2 μm buried oxide layer [8]. This SOI chip also has a 1.6 μm thick top oxide cladding. Figures 1(a) and 1(b) show a microscope picture of a typical AWG and PCG, also known as echelle grating, fabricated on a SOI chip. The design strategy for AWGs and PCGs is well known [9–11]. When the interest lies in a high-resolution spectrometer, AWGs are often preferred as the PCG performance generally decreases faster with increased resolution. This is a consequence of the larger physical delay length of the slab region in comparison with the delay wires of an AWG [4]. This leads to an increase in accumulated phase errors for a given resolution requirement. Figures 1(c) and 1(d) provide a diagram of respectively an AWG and PCG demultiplexer structures with all important dimensions indicated. To assess the performance
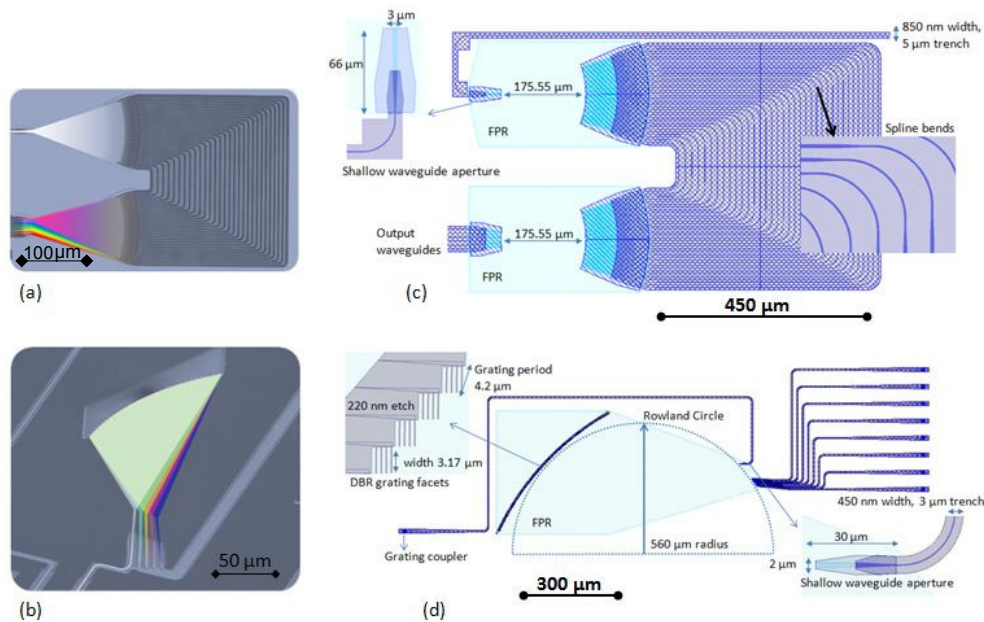

Fig. 1. Microscope picture of (a) an arrayed waveguide grating and (b) a planar concave grating illustrating the basic demultiplexer functionality. (c) schematic of the low resolution AWG design for 2200 nm and (d) schematic of the PCG with center wavelength of 1550 nm, both indicating the critical design parameters.

of the demultiplexers in the SWIR, we used an automatic alignment set-up combined with a pulsed supercontinuum laser as a broadband source (1900-2400 nm) and a optical spectrum analyzer (Yokogawa AQ6375) with an addressable wavelength range from 1200 nm to 2500 nm. The optical chip is accessed with single mode optical fibers through grating couplers for TE-polarized light. The grating coupler has 20 periods and consists of 220 nm deep trenches and is coupled to a 150 nm thick silicon waveguide. The grating period is 1.45 μm, 1.57 μm and 1.61 μm with a filling factor of 0.35, for a central wavelength of respectively 2.125 μm, 2.2 μm and 2.32 μm. The filling factor is the un-etched fraction of the grating. A linear taper is then used to convert the mode from the 150 nm thick waveguide to a standard 220 nm high silicon wire. The silicon wires have a propagation loss of 2.9 dB/cm at 1.55 μm and 1.15 dB/cm at 2.1 μm for a waveguide width of 450 nm and 850 nm respectively. These losses were measured using a cut-back method using four spiral waveguides with a length of 1 cm, 2 cm, 4 cm and 7 cm. For the assessment of the PCGs with 1.55 μm and 1.65 μm center wavelength, we utilize

the same optical set-up with an SLED and a polarizer before entering the chip through grating couplers with shallowly (70 nm) etched trenches. A grating period of 630 nm and 690 nm with a fill factor of 0.5 is used for a central wavelength of 1550 nm and 1650 nm. Table1 gives an overview of the specifications and device critical dimensions for the respective spectrometers.

Table 1. DESIGN PARAMETERS OF THE INDIVIDUAL DEMULTIPLEXERS

	AWG1	AWG2	PCG 1	PCG 2	PCG 3	PCG 4
center λ [nm]	2200	2200	1550	1650	2125	2320
resolution [nm]	1.6	4.8	3.2	7	6	5
number of channels	6	6	8	14	16	8
wire width [μm]	0.85	0.85	0.45	0.5	0.8	0.8
aperture width [μm]	3	3	2	2	3	3
free spectral range [nm]	13	38	115	121	150	60
DBR period [nm]	x	x	600	340	500	540
footprint [mm^2]	1.0	0.48	0.56	0.24	0.54	1.04

2.1. Arrayed waveguide grating

The arrayed waveguide gratings consist of two free propagation regions (FPR) and an array of waveguides with a constant length increment between them. Star couplers with shallowly etched (70 nm) apertures connect the input and output waveguides with the waveguide array. A double adiabatic taper converts the deeply etched photonic wires, used for routing, to the entrance and exit apertures. This approach reduces the index contrast between the waveguide apertures and the FPR. More information on the theory of AWG design can be found in [9]. In this work, a high resolution (100 GHz or 1.6 nm) and a low resolution (300 GHz or 4.8 nm) AWG were designed for TE polarized light with a center wavelength of 2.2 μm. The design strategy aimed at a small device size, resulting in a footprint of respectively, 1 mm^2 and 0.48 mm^2. Both AWGs have a set of 36 arrayed waveguides. In Fig. 2 the measured on-chip transmission spectra of the different demultiplexer designs is plotted. The high resolution AWG has an insertion loss of 4 dB and low crosstalk of -16 dB whereas the low resolution AWG has an insertion loss of 2.15 dB and a crosstalk level of -12 dB. The difference in insertion loss is mainly attributed to the difference in footprint. Good channel uniformity is obtained. Furthermore, this high performance is maintained over a wide wavelength range from 2.0 to 2.25 μm.

2.2. Planar concave gratings

The planar concave grating design is based on the Rowland geometry with one stigmatic point [10]. The entrance and exit waveguides with shallowly etched apertures are positioned along the Rowland circle with a radius R and the curved grating follows a circle with a radius of 2R. The PCGs are designed for TE polarization and have a grating with distributed Bragg reflector (DBR) facets. The use of DBR facets enhances the reflectivity of the grating, thus reducing the insertion loss [3]. In table 1 the design parameters of all PCGs are listed. The DBR grating is a second order grating in the case of PCG 1 and a first order grating in the case of PCG 2, PCG 3 and PCG 4. PCG 2 and 3 are targeted for the absorption spectrum measurement of biodiesel [12]. Both PCGs are preceded by a spiral waveguide of length 1.7 cm and 1 cm, for PCG 2 and PCG 3 respectively, that can be used for evanescent sensing [13]. In Fig. 2 the measured transmission of the different PCG designs is shown. In case the PCG is preceded by a spiral waveguide, the spiral insertion loss is not included in the plotted PCG transmission.

The insertion loss of -5 dB to -7 dB for PCG 1 and 2 is higher than expected, but SEM pictures revealed that the DBR facets were not fully etched. The strong non-uniformity in the channel response of PCG 2 is attributed to the automatic measurement set-up procedure which performs poorly when the transmitted power is low. For PCG 3 and 4 the high insertion loss, in comparison with state-of-the-art devices at 1550 nm, is mainly caused by a non-optimal waveguide width of 800 nm. Although the crosstalk is masked by the noise floor in most measurements, a low crosstalk of at least -16 dB is obtained for all PCG designs. This was one of the goals of the design strategy that we used. We tried to make the device as compact as possible to avoid phase errors in a large FPR.
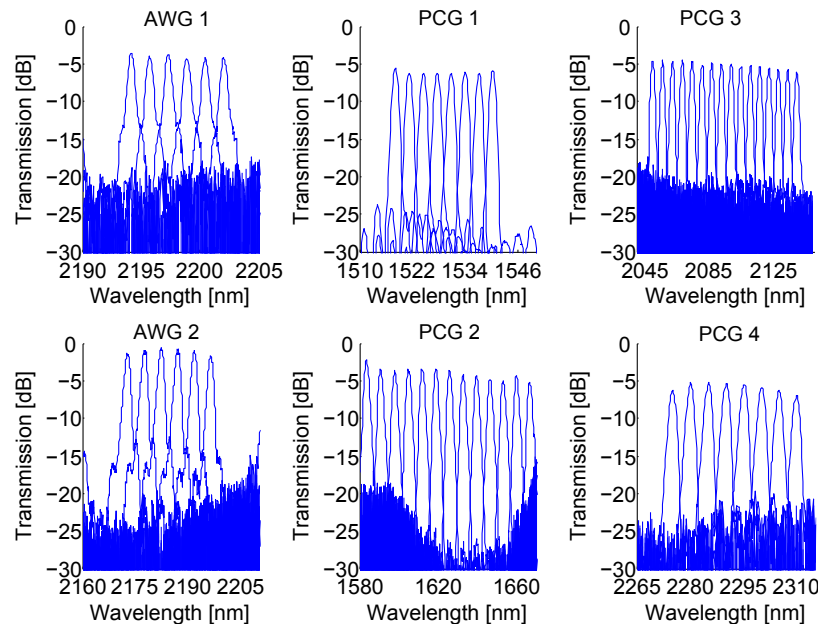
Fig. 2. Transmission of the different demultiplexer designs

3. Photodiode performance

The active photodetector material is a quaternary GaInAsSb epitaxial layer stack, grown by molecular beam epitaxy on a GaSb substrate [7]. This material, and GaSb compounds in general have proven to be excellent semiconductor materials for the short-wave infrared [14]. The used III-V epi-stack has a bandgap wavelength of 2.65 μm at room temperature. The layer stack used for the integrated photodetectors is shown in Fig. 3, together with a schematic of the grating-assisted coupling mechanism and scanning electron microscope picture of the cross-section of the integrated photodetector. The epitaxial stack is made using a reversed stack growth. It consists of a 50 nm thick p-doped (1.0×10^{18} cm^{-3}) GaSb and a 50 nm p-doped (1.0×10^{18} cm^{-3}) Ga$_{0.79}$In$_{0.21}$As$_{0.19}$Sb$_{0.81}$ layer as the p-zone of a p-i-n layer stack. A not intentionally doped 500 nm thick Ga$_{0.79}$In$_{0.21}$As$_{0.19}$Sb$_{0.81}$ layer is used for the intrinsic absorbing region. The n-type region consists of 80 nm Ga$_{0.79}$In$_{0.21}$As$_{0.19}$Sb$_{0.81}$ and 80 nm of InAs$_{0.91}$Sb$_{0.09}$. Both are doped to 1.0×10^{18} cm^{-3}. A grading layer of 40nm is used between Ga$_{0.79}$In$_{0.21}$As$_{0.19}$Sb$_{0.81}$ and InAs$_{0.91}$Sb$_{0.09}$. To integrate the p-i-n photodiodes onto the SOI chip, epitaxial layer transfer with DVS-BCB as bonding agent is carried out. The fabrication details of both the epi-stack and bonding procedure can be found in [7]. In this work, we opted for grating-assisted photode-

tectors as this relaxes the fabrication tolerances. In addition, we spaced the grating couplers at a comfortable distance of 75 μm to avoid crosstalk.
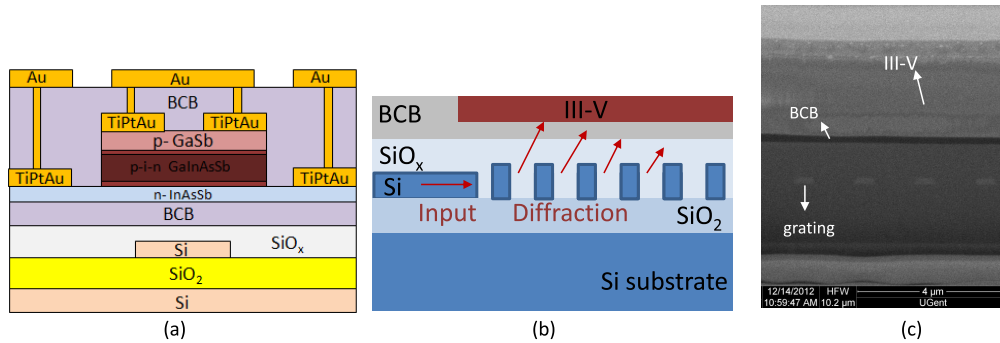

Fig. 3. (a) Layer stack used for the integrated photodetectors. (b) Schematic of the grating-assisted coupling mechanism. (c) SEM cross-section of the photodiode.

A total of 46 photodiodes were characterized with a failure of only 2 photodiodes. This proves the robustness of the fabrication process. The mean photodiode dark current at room temperature at a bias voltage of -1 V is around -2.5 μA for a mesa size of 17x50 μm^2 and -3 μA for a mesa size of 26x64 μm^2. For the optical characterization, light from a tunable laser is coupled to a single mode fiber and after passing a polarization controller this light was injected into the SOI circuit through grating couplers. In Fig. 4, I-V curves for a photodiode for various input power levels at a wavelength of 1530 nm are displayed. The input power as set in the top X-axis, is calibrated for polarization and on-chip losses (grating efficiency, waveguide loss and PCG/AWG insertion loss), whereas the inset contains the laser power before entering the optical chip. We obtain an on-chip responsivity of 0.61 A/W at the bias voltage of -0.5 V. A similar measurement was done at a wavelength of 2324 nm, resulting in an on-chip responsivity of 0.7 A/W at a bias voltage of -0.5 V.
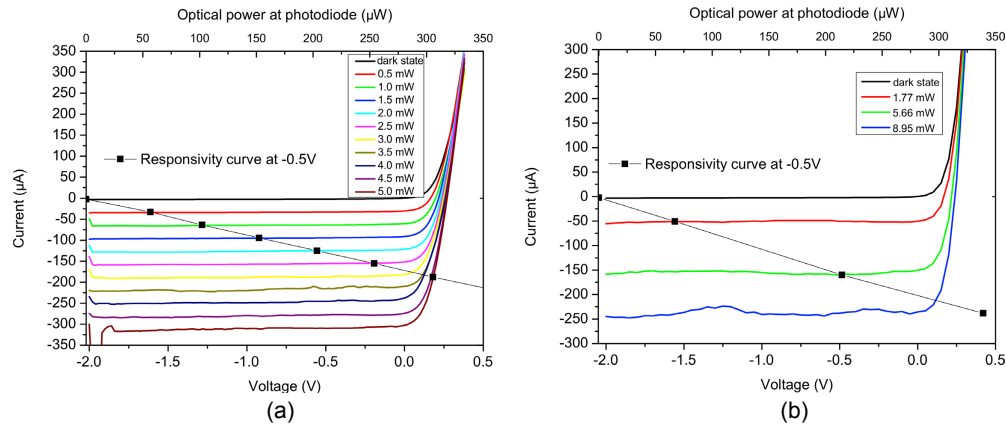

Fig. 4. IV-curves for a photodiode at a wavelength of 1530 nm (a) and 2324 nm (b) at different input power levels. The inset contains the laser power before entering the optical chip. The top X-axis refers to the optical power at the input of the grating coupler with integrated photodiode.
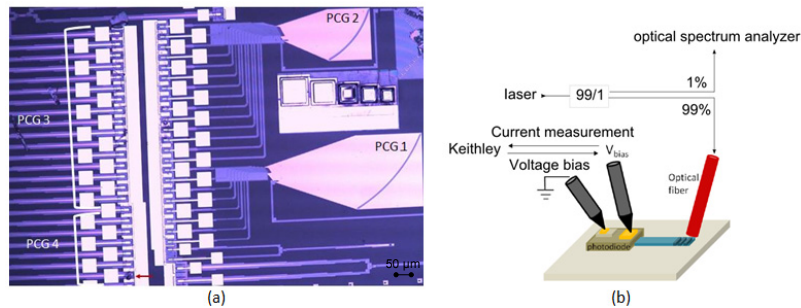
4. Spectrometer performance

Fig. 5. (a) Microscope picture showing the integrated photodiode array on top of the planar concave gratings. Only the PCGs with center wavelength of 1.55 μm and 1.65 μm (top right) are visible. The red arrow at the bottom indicates the single photodiode that failed during processing. (b) optical characterization set-up

Figure 5(a) is a microscope picture of the fabricated spectrometer chip. To characterize the spectrometers we use a set-up as shown in Fig. 5(b). Light from a laser source with tunable wavelength is split into two paths. A first path, with 1 percent of the input power, leads directly to an optical spectrum analyzer. For every lasing wavelength a spectrum is taken to obtain both a wavelength and power reference. The second path, with 99 percent of the input power, leads to the SOI chip comprising all four spectrometers. The photodetectors are individually probed for biasing and photocurrent read-out using a Keithley SourceMeter. The bias voltage is fixed at -0.1 V. For every spectrometer channel the laser is tuned with a wavelength step of 250 pm. A total of three different tunable lasers (TL) were needed to complete the measurement. For PCG1 and the first 7 channels of PCG 2 a Santec TL(1510-1630nm) is used. The remaining 7 channels of PCG 2 are measured with a Toptica DL100pro TL (1600-1750nm). Both PCG 3 and 4 are measured with a SFTL-Cr-ZnS/Se-2300-5000 TL from IPG Photonics (2000-2400nm). At the shorter wavelengths (2000-2050 nm), this laser is unstable on a time-scale shorter than the OSA spectrum acquisition time, therefore impacting the smoothness of the photocurrent measurement. In Fig. 6 the results of the electro-optical characterization is shown. All measurements were carried out at room temperature. Remark that it is a different SOI chip than the one used for the passive demultiplexer characterization in section 2, therefore an exact comparison of the losses was not possible. The photo-current is corrected for the input grating coupler and calibrated for a constant injected power of 1 mW at all wavelengths. The losses in the spiral waveguide, that preceeds PCG 2 and PCG 3, are not corrected for. Thus, the resulting photo-current is the photo-current that is measured when a constant input power of 1 mW at the entrance waveguide goes through the spiral waveguide and PCG to the photodetector. The rms dark current of the respective photodetectors is indicated by the green line. We note two outliers. The first outlier is the fifth photodiode of PCG 2. It has a very high dark current (>1000 μA) but is clearly responsive to light. It was added to the graph by reducing its photoresponse value by 1000 μA. The second outlier is the seventh photodiode from PCG 4, which behaves as an open circuit. The performance of PCG1, 3, 4 is similar, whereas PCG 2 has a lower photocurrent. We attribute this to the preceding spiral waveguide that was slightly damaged during fabrication. Although care was taken to provide a proper calibration, there is an amplitude discrepancy between the channels measured with the Santec TL and the Toptica TL. This is due to a slight deviation in the optical set-up between both measurements. The dark current at the low bias voltage of -0.1V is generally constant and below 2μA over the whole

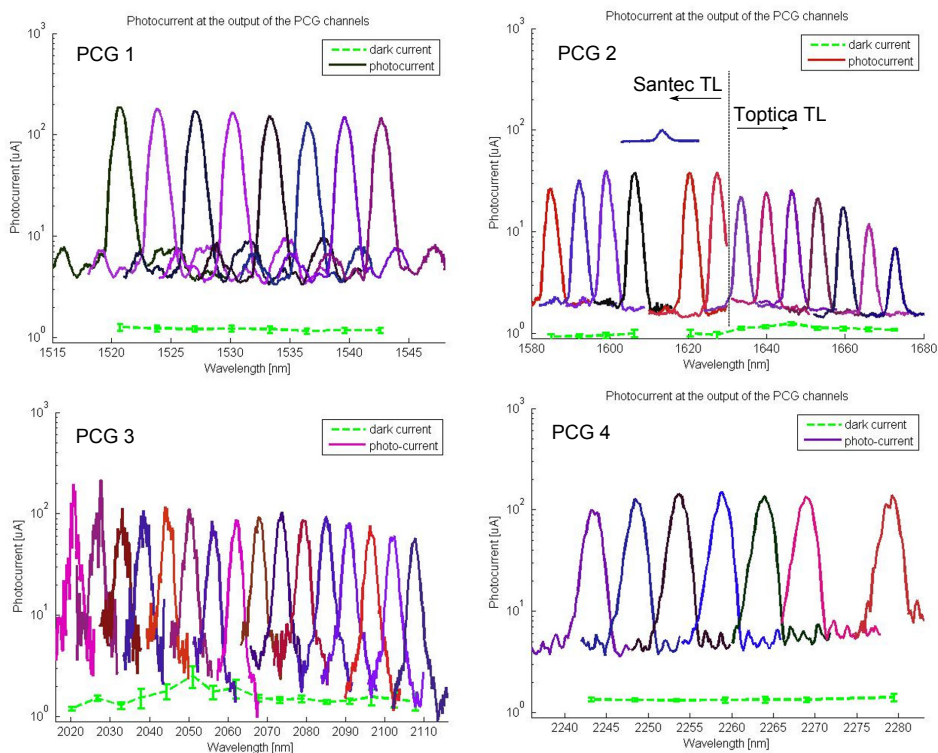wavelength range. A maximum crosstalk level of -10 dB is obtained for all spectrometers.

Fig. 6. Measurement result of the four planar concave gratings with integrated photodetectors. The curves represent the photocurrent that is obtained when 1 mW is injected in the entrance waveguide and after transmission through the waveguide spiral and PCG.

5. Conclusion

We presented the integration of spectrometers on the silicon-on-insulator platform with operating wavelengths from the telecommunication band to the short-wave infrared. The optical characterization of the demultiplexer designs showed a modest insertion loss of -5 dB while keeping low crosstalk over a variety of wavelengths and spectral resolutions. On top of the output grating couplers of the planar concave gratings, an array of GaInAsSb photodiodes was fabricated. A dark current of -2.5 μA at a bias voltage of -1 V and responsivity values at a bias of -0.5 V of 0.61 A/W at 1530 nm and 0.7 A/W at 2200 nm were obtained. Care was taken to maintain a low channel crosstalk after photodiode integration. A high performance of each of the spectrometers at the four selected wavelength ranges was obtained. Future work will be focused on performing evanescent absorption spectroscopy with these integrated devices. An additional integration step with micro-fluidics will then lead to a truly on-chip spectrometer.